AGU PUBLICATIONS

JGR

Journal of Geophysical Research: Atmospheres

RESEARCH ARTICLE
10.1002/2016JD024820

Key Points:
- The 23-30 January 2012 SPE caused an ~10% increase in PMCs mass seen by AIM and predicted by WACCM
- PMC increase is opposite in sign to the SPE effects previously reported
- Water vapor in the sublimation area may be a better indicator than ice mass of SPE effects on PMC

Correspondence to:
C. G. Bardeen,
bardeenc@ucar.edu

Citation:
Bardeen, C. G., D. R. Marsh, C. H. Jackman, M. E. Hervig, and C. E. Randall (2016), Impact of the January 2012 solar proton event on polar mesospheric clouds, *J. Geophys. Res. Atmos.*, *121*, 9165–9173, doi:10.1002/2016JD024820.

Received 19 JAN 2016
Accepted 22 JUL 2016
Accepted article online 25 JUL 2016
Published online 12 AUG 2016

Impact of the January 2012 solar proton event on polar mesospheric clouds

C. G. Bardeen[1], D. R. Marsh[1], C. H. Jackman[2], M. E. Hervig[3], and C. E. Randall[4]

[1]National Center for Atmospheric Research, Boulder, Colorado, USA, [2]Emeritus, NASA Goddard Space Flight Center, Greenbelt, Maryland, USA, [3]GATS, Inc., Driggs, Idaho, USA, [4]Laboratory for Atmospheric and Space Physics and Department of Atmospheric and Oceanic Sciences, University of Colorado Boulder, Boulder, Colorado, USA

Abstract We use data from the Aeronomy of Ice in the Mesosphere mission and simulations using the Whole Atmosphere Community Climate Model to determine the impact of the 23–30 January 2012 solar proton event (SPE) on polar mesospheric clouds (PMCs) and mesospheric water vapor. We see a small heating and loss of ice mass on 26 January that is consistent with prior results but is not statistically significant. We also find a previously unreported but statistically significant ~10% increase in ice mass and in water vapor in the sublimation area in the model that occurs in the 7 to 14 days following the start of the event. The magnitude of the response to the January 2012 SPE is small compared to other sources of variability like gravity waves and planetary waves; however, sensitivity tests suggest that with larger SPEs this delayed increase in ice mass will increase, while there is little change in the loss of ice mass early in the event. The PMC response to SPEs in models is dependent on the gravity wave parameterization, and temperature anomalies from SPEs may be useful in evaluating and tuning gravity wave parameterizations.

1. Introduction

The solar proton event (SPE) of 23–30 January 2012 is one of the two largest in solar cycle 24 and is one of the 12 largest in the last 50 years [*Jackman et al.,* 2014]. Ionization of the atmosphere by solar protons results in an increase in HO_x (H, OH, and HO_2) [*Swider and Keneshea*, 1973] and NO_x (N, NO, and NO_2) [*Crutzen et al.,* 1975], which in turn can cause catalytic destruction of ozone [*Weeks et al.,* 1972; *Solomon and Crutzen*, 1981]. Observations of the January 2012 SPE from the Michelson Interferometer for Passive Atmospheric Sounding (MIPAS) show an increase in HO_x and NO_x and a decrease in ozone in the polar stratosphere and mesosphere [*von Clarmann et al.,* 2013]. *Jackman et al.* [2014] also found increases in HO_x and decreases in ozone using data from the Microwave Limb Sounder (MLS) for the same time period. They also modeled the effects of this SPE using the Goddard Space Flight Center (GSFC) two-dimensional model and found good agreement with the MLS and MIPAS observations. Based upon simulations with and without the SPE, they attributed the changes in HO_x, NO_x, and ozone to the SPE.

Changes in ozone will cause changes in temperature, where lower ozone corresponds to less heating from solar absorption and thus lower temperatures in the sunlit upper stratosphere and lower mesosphere. Dynamical changes driven by this cooling in the lower mesosphere will modulate gravity wave fluxes and induce a reduced upwelling causing less adiabatic cooling (a relative warming) during the polar summer in the upper mesosphere and lower thermosphere, while Joule and chemical heating have only small effects in the summer mesosphere [*Jackman et al.,* 2007]. Simulations by *Becker and von Savigny* [2010] indicate that the ozone cooling in the lower polar mesosphere causes changes to zonal winds and a reduction in gravity wave drag that reduces upwelling in the polar summer mesosphere resulting in less cooling (relative heating) compared to the case without the ozone cooling. The GSFC model used by *Jackman et al.* [2014] predicts a 0.8 K warming in the upper mesosphere and a 1 K cooling in the upper stratosphere and lower mesosphere for the January 2012 SPE. If an SPE occurs during the polar summer, when polar mesospheric clouds (PMCs), also known as noctilucent clouds, are present, these temperature changes may cause changes in the clouds. *Von Savigny et al.* [2007] found that during the January 2005 SPE there was up to a 12 K increase in upper mesospheric temperature as measured by MLS and a 60% decrease in PMC frequency as measured by the Scanning Imaging Absorption Spectrometer for Atmospheric Chartography. To extend this result to other years, *Rahpoe et al.* [2011] looked for correlations in 30 years of the Geostationary Operational Environmental Satellites (GOES) solar proton fluxes and the Solar Backscatter Ultraviolet (SBUV) PMC frequencies and albedos. They found weak negative correlations with a lag of 0 to 8 days in agreement with the result of *von Savigny et al.* [2007]. *Winkler*

et al. [2012] used a one-dimensional model forced by MLS temperatures and water vapor to study the effects of the January 2005 SPE. They included the effects of ionization from the SPE and subsequent proton hydrate chemistry depleting water vapor, which they found to have a minimal impact, but did not include the ionization effects causing ozone depletion and subsequent changes in temperature.

Here we look for signatures of the 23–30 January 2012 SPE in PMCs using the Whole Atmosphere Community Climate Model (WACCM) [*Garcia et al.,* 2007; *Marsh et al.,* 2013] and data from the Aeronomy of Ice in the Mesosphere (AIM) [*Russell et al.,* 2009] mission. Section 2 describes the WACCM model configuration, while section 3 introduces the AIM data sets used for the analysis. Model results and comparisons with the AIM data are presented in section 4, followed by a summary and discussion of the implications of these results in section 5, and then concluding remarks in section 6.

2. Model

WACCM is the high-top variant of the Community Earth System Model, (CESM) [*Hurrell et al.,* 2013] from the National Center for Atmospheric Research (NCAR) that extends to ~140 km and includes coupled photochemistry. WACCM includes a parameterization that takes ionization rates derived from proton fluxes measured by GOES and converts them into HO_x and NO_x production rates as described in *Jackman et al.* [2008]. WACCM does not include a parameterization for PMCs, so we couple WACCM with the Community Aerosol and Radiation Model for Atmospheres (CARMA) [*Toon et al.,* 1988; *Bardeen et al.,* 2008, 2010], a sectional cloud and aerosol parameterization, to represent PMC ice particles and the meteor smoke particles upon which they nucleate. We used a similar WACCM/CARMA configuration with version 3 of WACCM [*Bardeen et al.,* 2010], but now use this with version 4 of WACCM. *Marsh et al.* [2013] describe the differences between WACCM3 and WACCM4. WACCM4 offers several improvements over WACCM3 including $1.9° \times 2.5°$ horizontal resolution, support for running the model for historical time periods by nudging the model state to reanalysis meteorology [*Lamarque et al.,* 2011], and output of model data at high temporal resolution along prescribed satellite tracks. WACCM4 does introduce a new gravity wave parameterization; however, since PMCs are very sensitive to the gravity wave parameterization, we have reverted to the WACCM3 gravity wave parameterization tuned similarly to *Bardeen et al.* [2010]. As in *Bardeen et al.* [2010], vertical levels have been added providing ~300 m resolution in the mesosphere to better resolve the PMC structure. To simulate 2012 conditions, GEOS5-data assimilation system reanalysis data V5.2 [*Rienecker et al.,* 2008] is used to nudge the winds and temperature in the model using an ~100 h relaxation time scale; the nudging is fully applied below 20 km tapering off to no nudging above 30 km. This is done not only to recreate the historical state in the troposphere but to still allow the winds and temperatures to respond to the changes caused by the SPE in the upper stratosphere and mesosphere.

3. Instruments

The AIM satellite has two instruments designed to characterize PMCs: the Cloud Imaging and Particle Size (CIPS) [*McClintock et al.,* 2009] experiment and the Solar Occultation For Ice Experiment (SOFIE) [*Gordley et al.,* 2009]. CIPS is an ultraviolet imager that measures scattered radiation at 265 nm with four nadir cameras that acquire successive measurements of the same location at approximately seven different scattering angles. The CIPS horizontal resolution is 25 km^2, and each four-camera image covers an area of roughly 1000 km (cross track) by 2000 km (along track). We use the ice water content (IWC) from the V4.20 CIPS data [*Lumpe et al.,* 2013] summed daily, to provide a daily measurement of the total PMC ice mass. CIPS provides IWC covering the polar cap, generally between about 60° and 85°. SOFIE is a solar occultation instrument that yields vertical profiles of temperature, the abundance of five gaseous species (O_3, H_2O, CO_2, CH_4, and NO), PMCs, and meteoric smoke [*Gordley et al.,* 2009; *Hervig et al.,* 2009a, 2009b] with ~1.8 km vertical resolution. SOFIE determines a variety of PMC properties including ice mass density (M_{ice}), vertical column ice water content (IWC), and the ice particle shape, size, and concentration [*Hervig et al.,* 2009a]. Observations are taken continuously at latitudes from 65° to 82°S (spacecraft sunset) and 65° to 82°N (sunrise), essentially following the latitude of the day-night terminator with season. We use V1.3 SOFIE data, and for model comparisons WACCM/CARMA is sampled at the same time and location as the SOFIE measurements. For a more detailed discussion of comparing CIPS and SOFIE data with results from the WACCM/CARMA model see *Bardeen et al.* [2010].

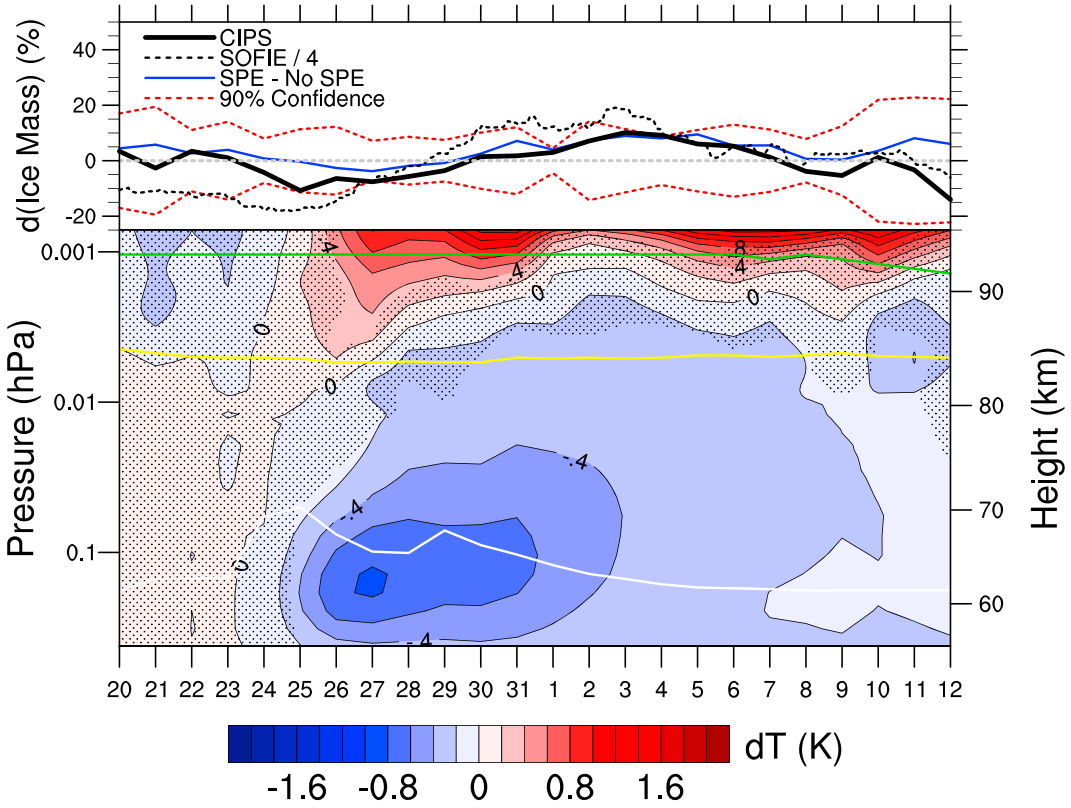

Figure 1. Evolution of the SH polar cap (60°S to 90°S) daily average difference between the SPE and No SPE simulations from 20 January 2012 to 12 February 2012 for (top) total PMC ice mass (blue line) and (bottom) temperature. Also shown are the anomaly for this period in CIPS total ice mass (top, solid black line), SOFIE total column ice mass density (top, dotted black line), and the 90% confidence level from the No SPE ensemble (top, red lines). The CIPS and SOFIE data have been smoothed with a 5 day running average. The lines in the temperature plot indicate the average mesopause height (green), the average height of the maximum PMC ice mass density (yellow), and the computed SPE-induced ionization rate at 0.1 hPa (white) from the SPE simulations. The ionization rate is provided to give a qualitative indication of the timing of the event, and thus, no scale is provided. The percentage change in SOFIE ice mass density has been scaled down by a factor of 4 so that it will fit onto the same plot as the CIPS and WACCM/CARMA results.

4. Results

We conducted three 6-member ensemble simulations: (1) with no solar proton forcing (No SPE); (2) with the observed forcing (SPE); and (3) with the forcing from 2012 replaced with the forcing from the 2003 "Halloween Storms" (SPEHW). The Halloween Storms are the fourth largest SPE in the last 50 years [*Jackman et al.,* 2008]. Relative to the January 2012 SPE, they have increased ionization and are "harder" meaning that a greater fraction of the particles have higher energies and therefore increase ionization at lower altitudes. Averages and variances are calculated for each of the ensembles. Additionally, two simulations were done with twice (SPE2HW) and 4 times (SPE4HW) the forcing from the Halloween Storms.

First, we will look at results from the WACCM/CARMA simulations. Figure 1 shows the difference of the SH polar cap (60°S–90°S) daily average total ice mass (top) and temperature (bottom) between the SPE and No SPE ensemble averages from 20 January 2012 to 12 February 2012. The shading in the temperature plot indicates areas where the temperatures in the SPE ensemble are not significantly different, to the 90% confidence level, from the No SPE ensemble. The white line indicates the SPE ionization rate at 0.1 hPa used by the model, which ranges from 0.8 to 2485 ion pairs $cm^{-3}\,s^{-1}$. The yellow line indicates the PMC cloud height, the altitude where the maximum ice mass density occurs. The green line indicates the height of the mesopause, the altitude with the minimum average temperature. During this time period WACCM/CARMA has an average mesopause temperature of 128 K. Cooling at ~60 km caused by the SPE starts on 23 January because of ozone destruction and maximizes at 0.8 K on 27 January when cooling also begins at PMC

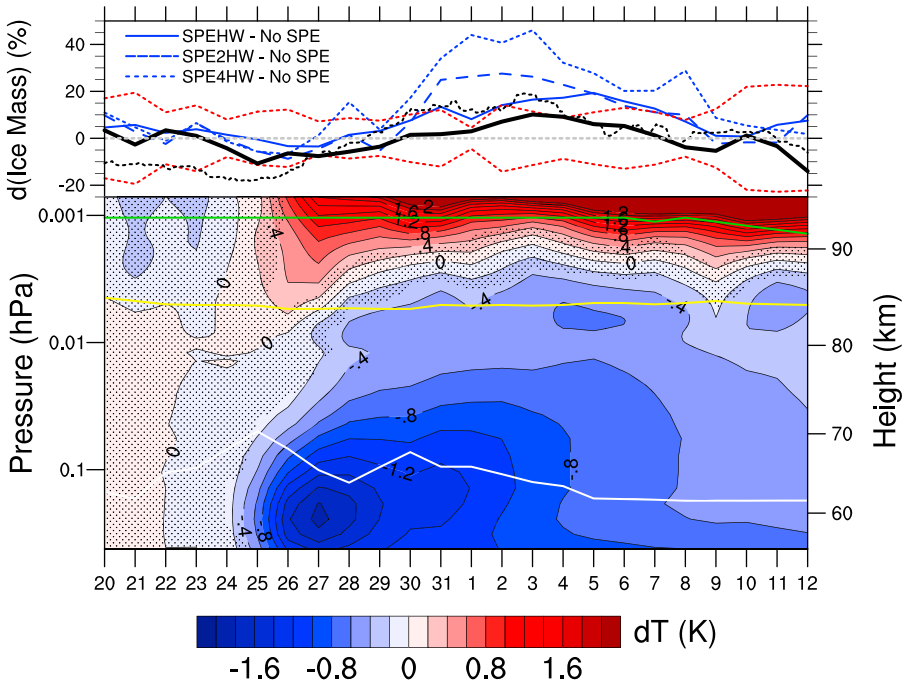

Figure 2. Similar to Figure 1 for the simulations where the SPE ionization rates for this time period have been replaced with scaled amounts from the 2003 Halloween storm. Ice mass are shown for 1 times (solid blue line), 2 times (dashed blue line), and 4 times (dotted blue line) the Halloween forcing. The temperatures are from the 1 times case. The solid black (CIPS anomaly), dotted black (SOFIE anomaly), green (mesopause), yellow (maximum PMC ice density), white (ionization rate) and red (90% confidence level) lines are as in Figure 1.

altitudes. Cooling at cloud height is greater than 0.2 K from 28 January to 8 February and is significant over most of that period. Heating occurs at cloud height on 23 January but is only statistically significant beginning on 26 January above the cloud height. Heating is caused by reduced gravity wave drag and therefore reduced upwelling and reduced adiabatic cooling giving a relative heating. The difference in ice mass between the SPE and No SPE ensembles (blue line) shows a 5% decrease on 27 January, followed by a longer period of up to a 10% increase starting on 29 January and lasting to 8 February. This model result is in good agreement with the CIPS observed anomaly for 20 January to 12 February, calculated from the average over the same time period, from the CIPS total ice mass (solid black line) smoothed with a 5 day running average to minimize the effects of other sources of variability like planetary waves. The same general pattern is also seen in the anomaly in the SOFIE total ice mass density calculated in the same way and also smoothed over 5 days (dotted black line); however, the variability is much larger. The value shown in Figure 1 for SOFIE is reduced by a factor of 4 to fit into the plot. Each day SOFIE makes 15 observations at one latitude per hemisphere, so it is not surprising that it would have higher variability than the changes seen in CIPS and the model that are using polar cap averages for each day.

While there is a small, but significant cooling response in temperature at cloud height from the 2012 SPE, the response in total ice mass only just reaches the significance level for 1 day. The dotted red lines in Figure 1 indicate the 90% confidence level for the total ice mass anomaly in the SPE ensemble compared to the No SPE ensemble using a Student's *t* test. To explore the response of the model to larger SPEs, the ionization rates for the 20 days centered on the strongest rate in the 23–30 January 2012 SPE are replaced with the rates from the 20 days centered on the peak of the 2003 Halloween Storms. Figure 2 shows a plot similar to Figure 1 for the difference in total ice mass and temperature between the SPEHW and No SPE cases. For the Halloween Storms, the maximum ionization rate is 8215 ion pairs $cm^{-3}\,s^{-1}$ at 1 hPa. The temperature differences are larger than those in Figure 1, but at cloud height the heating is still not significant, and the cooling has increased to greater than 0.4 K between 29 January and 8 February for the SPEHW case, ~0.6 K for the SPE2HW case (not shown) and ~1.0 K for the SPE4HW case (not shown). There is a small but still insignificant decrease in ice mass early in the event, but the later cooling now causes a significant increase in ice mass for

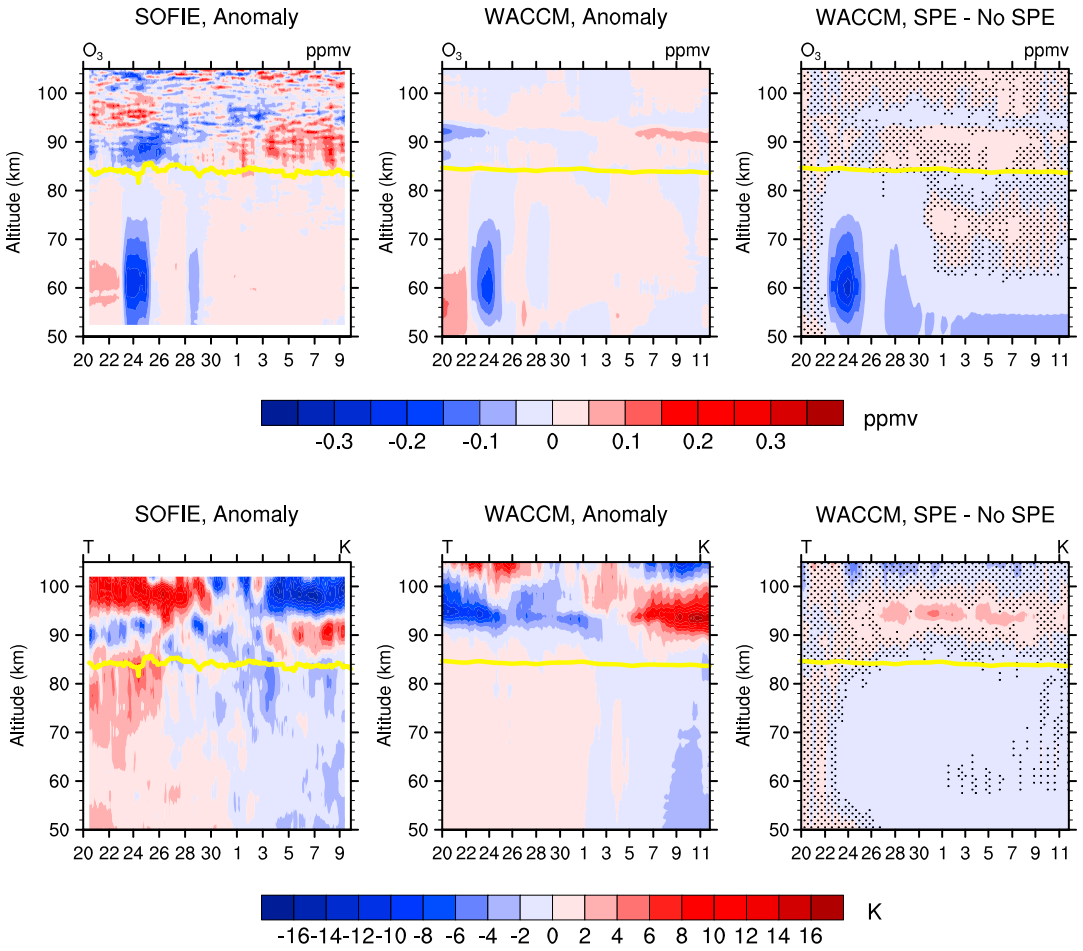

Figure 3. Evolution of (top row) ozone and (bottom row) temperature anomalies from (left column) SOFIE and the (middle column) SPE simulations along with evolution of the difference between the (right column) SPE and No SPE simulations for the period 20 January 2012 to 12 February 2012. Data from the model are sampled at the SOFIE locations and times, and all plots are smoothed with a 15-event (daily) running average. In all panels, the yellow line is the altitude of peak PMC ice mass density. In Figure 3 (right column), the shading indicates areas where the difference is not significant at the 90% level compared to the variability in the No SPE simulations.

several days with a maximum increase of 20% in the SPEHW case (solid blue line), 25% in the SPE2HW case (dashed blue line), and 45% in the SPE4HW case (dotted blue line).

Comparisons of the WACCM simulations with SOFIE data allow for the evaluation of the vertical structure of ozone, temperature, ice mass, and water vapor. Figure 3 shows the evolution of the vertical profiles of ozone (top row) and temperature (bottom row) from SOFIE and the model. For SOFIE (left), the anomaly for 20 January to 12 February, calculated from the average over the same time 23 day period, smoothed by a 15-event (daily) running average is plotted. For the model, the anomaly from the SPE case is plotted in the same way as the SOFIE data (center), and the difference between the SPE and No SPE cases is also plotted using a 15-event running average (right). The two anomaly plots allow the model and the data to be compared directly, while the SPE-No SPE plot indicates how much of the anomaly can be attributed to the 2012 SPE. The model winds and temperatures are nudged to meteorology below 30 km but are free running in the region of interest, so we do not expect the variability in SOFIE and WACCM in the mesosphere to be the same. SOFIE measured two major ozone depletion events of ~0.24 ppmv on 24 January and ~0.06 ppmv on 28 January near 60 km where the maximum cooling occurs. The model result is shifted early by 12 h because of an error in specifying the time of the daily average SPE ionization rates and has a slightly smaller depletion (~0.2 ppmv and ~0.05 ppmv, respectively). This error has since been fixed; however, it is not expected to have a significant effect on the results so we did not repeat the simulations. SOFIE shows more variability in ozone above

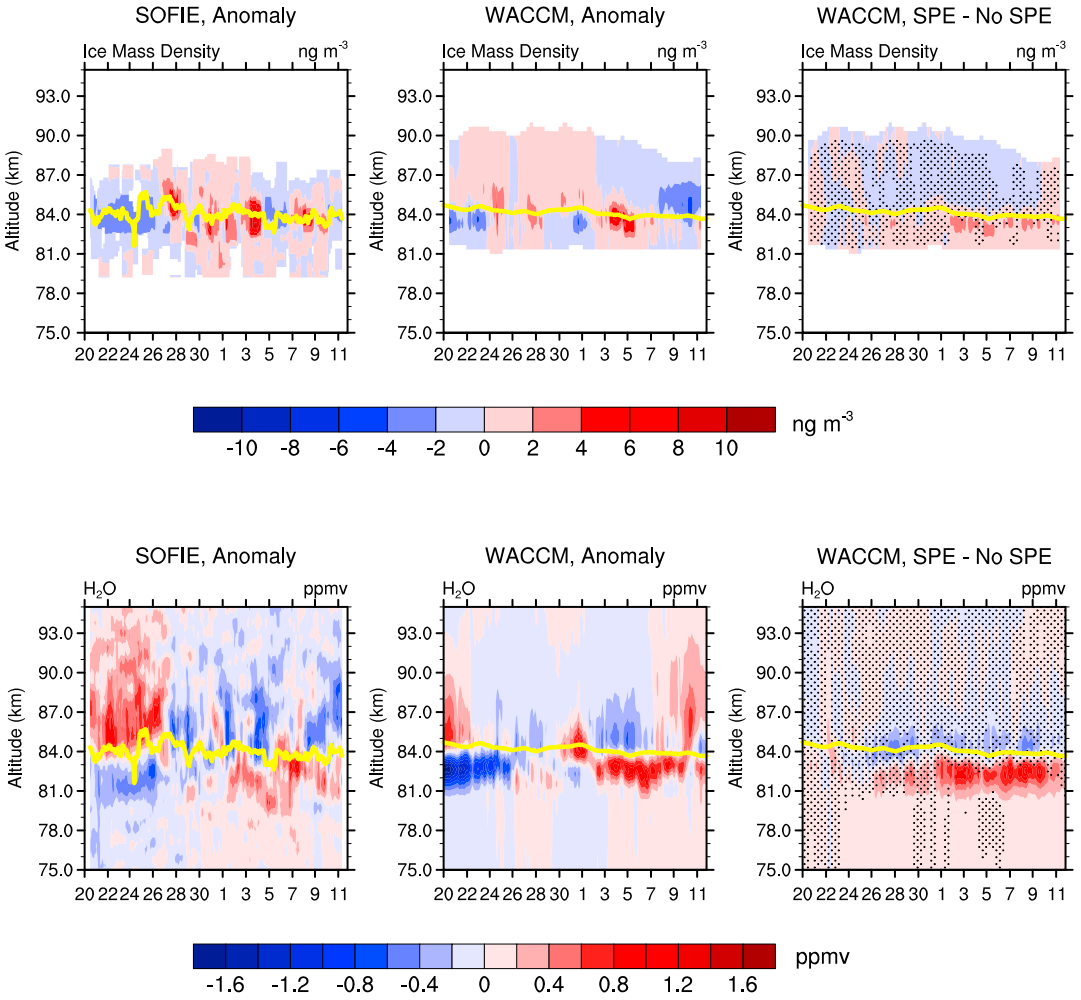

Figure 4. Similar to Figure 3 but for (top row) ice mass density and (bottom row) water vapor.

85 km than the model including a loss near 90 km at the beginning of the time period and a gain at the end that is also present in the WACCM anomaly, but this does not appear to be caused by the SPE. Large temperature anomalies exist in the upper mesosphere and lower thermosphere above cloud level, going from cooling in the first half of the time period to heating in the second half for both the data and the model. The altitude of the peak in the heating anomaly is ~5 km higher in WACCM than in SOFIE and has broader vertical extent, covering ~10 km in the model and ~5 km in the data. This heating comes from changes in gravity wave-driven upwelling, suggesting a bias in the gravity wave parameterization in the model. The model gravity waves were tuned to give cloud heights and cloud mass that are in agreement with observations for 2007 and 2008, and there is good agreement in cloud heights for January to February 2012. SOFIE and WACCM/CARMA anomalies both show a transition from warming to cooling at cloud level and below, and the SPE-No SPE difference plot indicates that some of this cooling is caused by the SPE. Comparing Figure 1 and Figure 3 shows that the maximum cooling is in the same area as the maximum SPE-induced ozone destruction.

Figure 4 is similar to Figure 3 but shows vertical profiles of ice mass density (top row) and water vapor (bottom row). The anomalies in ice mass are different between SOFIE and WACCM, suggesting that sources of variability like gravity waves [*Rapp et al.,* 2002] and 2 day and 5 day planetary waves [*Merkel et al.,* 2003; *Dalin et al.,* 2011] not reproduced identically in the model have a larger effect on daily ice mass than the SPE. In general, there does appear to be an increase in ice mass over the period of SPE-induced cooling, but in Figure 4 it is difficult to discern over the background variability. However, Figure 1 did show an increase in ice mass from SOFIE for this period. The SPE-No SPE difference shows an increase in ice at or just below

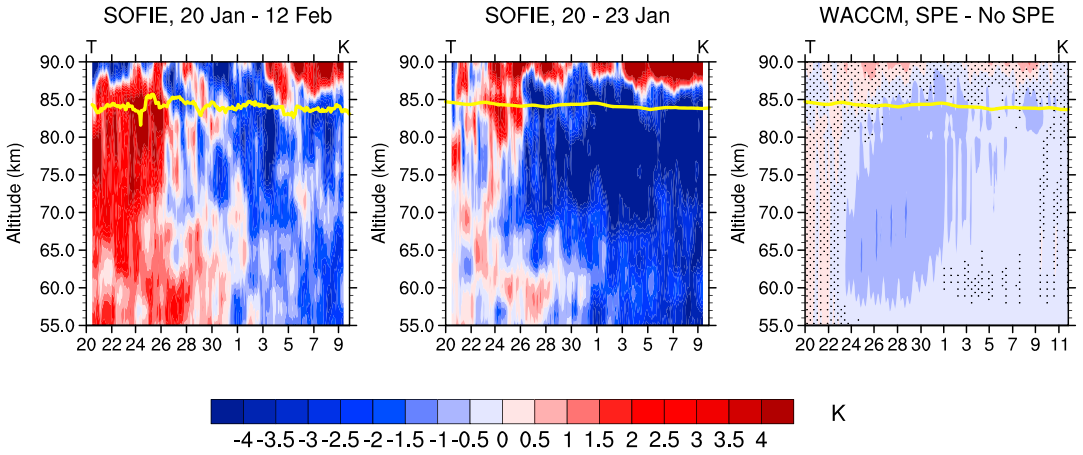

Figure 5. Similar to Figure 3 but over a smaller altitude range, with an expanded temperature scale, and with the WACCM anomaly plot replaced by another version of the SOFIE anomaly plot. The SOFIE anomaly plot in the center is the anomaly compared to the average over 20–23 January, rather than the average over the period from 20 January to 12 February.

cloud level that is significant to the 90% level from 1 to 10 February; however, this difference is smaller in magnitude than the variability suggested by the anomalies. Water vapor shows better agreement between the SOFIE and WACCM anomalies, and much of the anomaly can be attributed to the SPE. There is a decrease in water vapor at and above cloud level where clouds are growing and depleting the vapor, while there is an increase in water vapor in the region below cloud level caused by the sublimation of a larger mass of cloud. The decreases in water vapor above cloud level vary opposite to the variability in the ice mass, so it is also responding to other forms of variability that affects the ice. For example, in the SOFIE data there are positive water vapor anomalies at or above cloud level from 20 to 27 January and 5 to 7 February corresponding with decreases in ice mass, and negative water vapor anomalies from 27 to 30 January and 7 to 9 February corresponding with increases in ice mass. Water vapor in the sublimation region increases throughout the event, where water vapor is building up from sedimentation and sublimation of the generally increased ice mass. Thus, water vapor in the sublimation region, which is effectively an integral of the changes in the ice mass over this time period, may be the most sensitive indicator of SPE effects on PMCs; however, the water vapor observations must have sufficient vertical resolution (~1 km) to separate the decrease at and above cloud level from the increase below.

Figure 5 shows a temperature plot similar to Figure 3; however, the altitude range has been limited to the mesosphere, the temperature contours are more tightly spaced, and the WACCM anomaly plot has been replaced by a second SOFIE anomaly plot that uses the average over the time period before the SPE (20–23 January) as the reference temperature for the anomaly calculation. While there is a lot of background temperature variability and a strong background cooling trend over this time period, there is an indication in the SOFIE data of the SPE-induced cooling that is seen in the WACCM/CARMA SPE-No SPE result. This is particularly apparent in the center panel, where there is a somewhat "c" shaped pattern showing a transition from warm anomalies to cold anomalies from 23 to 28 January in the location and time predicted by the model for the onset of SPE-induced cooling. This cooling starts on 24 January at ~65 km and spreads out propagating upward and slightly downward over the next week. While not conclusive, this may be the first observation of SPE-induced cooling due to reduced adiabatic heating.

5. Discussion

Previous attempts to identify effects of SPE on PMCs [*von Savigny et al.*, 2007; *Rahpoe et al.*, 2011] have generally found heating that caused a reduction in cloud during the event. We find that for the 23–30 January 2012 SPE event the heating effect is minimal, but there is a prolonged cooling at cloud level that produces a significant increase in ice mass and water vapor in both the model and the observations. *Rahpoe et al.* [2011] did look for positive correlations between SPE and SBUV cloud frequency; however, they were unable to find a consistent positive correlation. This may have been because of the insensitivity of SBUV, the small sample size, and the

large natural variability. Increasing the averaging to smooth out the natural variability may allow for a positive correlation to be found, but we would expect it to be spread out and not to be sharply peaked at any particular lag. In our experiments, larger SPEs did not show a significant change in the cloud loss early in the event; however, they did show a large and significant increase in PMCs from the later cooling. SPE-caused increases in PMCs may be easier to detect if larger SPEs occur during the PMC season.

Our results show that the cloud altitude is above the area of maximum SPE-induced cooling and below the area of the maximum dynamical heating, suggesting that PMCs are not sensitive to the largest temperature changes induced by SPEs. *Von Savigny et al.* [2007] found an increase in MLS temperatures at 85 km during the January 2005 SPE; however, at this altitude MLS has a vertical resolution of ~14 km [*Schwartz et al.,* 2008]. Thus, MLS would be unable to determine whether the dynamical heating occurred at cloud level, as is assumed by *von Savigny et al.* [2007] and suggested by GSFC 2-D model for 2012 or above cloud level as observed by SOFIE and suggested by the WACCM/CARMA model for 2012. *Becker and von Savigny* [2010] suggest that their results are consistent with a heating-induced reduction in PMCs; however, their results also show the heating occurring above the cloud level, in a region from 85 to 100 km, along with a small cooling at cloud level consistent with our results. The level where dynamical heating occurs in the model is sensitive to the gravity wave parameterization; however, the gravity wave-induced upwelling is responsible for creating the cold summer mesopause and the largest upwelling and changes in that upwelling are above the mesopause. The warm temperature anomaly observed by SOFIE occurs at a lower altitude, covers a smaller altitude range, and has a smaller magnitude than in our WACCM/CARMA or the *Becker and von Savigny* [2010] simulations. These differences may be useful for evaluating and tuning gravity wave parameterizations. Observations with high vertical resolution like those from SOFIE are needed to determine whether there is heating or cooling at cloud level. The energy spectrum of an SPE will also affect the temperature response to the SPE, where an SPE with an equivalent total proton flux, but with more low energy and fewer high-energy particles would be expected to cause less ozone destruction and less cooling in the lower mesosphere. Such an SPE might also cause more heating near cloud level through Joule and direct particle heating.

While WACCM/CARMA indicates that SPEs cause a significant increase in cloud ice mass, there is a large amount of natural variability caused by gravity waves and planetary waves that is larger than the SPE-induced variability. This makes it difficult to identify SPE-induced changes in ice mass observations, particularly the heating-induced changes that are of short duration. Water vapor in the altitude range where the clouds are sublimating shows a larger and more consistent increase than is seen in the clouds. The water vapor continues to increase during the event, acting roughly as an integral of the ice changes over the time period. Simulations by *Winkler et al.* [2012] also showed a significant change in water vapor in the sublimation area following the January 2005 SPE; however, they were not matched by the available MLS and MIPAS observations. *Winkler et al.* [2012] assumed MLS temperatures and thus predicated a decrease in PMC and a decrease in water vapor at the sublimation area opposite to our results for the January 2012 SPE. Thus, water vapor may be a more sensitive indicator of the impact of SPEs upon PMCs; however, the observation needs to have a high vertical resolution. The vertical extent of the sublimation area is about 2 km and is adjacent to an area at and above the cloud level where the change is of opposite sign. The vertical resolution of the observations must be sufficient to resolve these two areas, as they will tend to cancel out if averaged together.

6. Conclusion

Using AIM data and the WACCM/CARMA model, we have found an SPE-induced cooling that increases PMCs in the 2 weeks following the January 2012 SPE. This is opposite in sign and occurs many days later than the SPE response seen by *von Savigny et al.* [2007] for the January 2005 SPE. We do see suggestions of a small heating and loss of PMCs early in the event consistent with *von Savigny et al.* [2007] and *Raphoe et al.* [Rahpoe *et al.,* 2011]; however, our result is not statistically significant and does not increase as the size of the SPE is increased. SOFIE does suggest a larger heating anomaly on 26 January than is seen in WACCM/CARMA, so perhaps a heating term is missing from the model or a slightly different gravity wave tuning might produce a larger heating and reduction in ice mass. The SOFIE temperature data may show the signature of an SPE-induced cooling in the mesosphere; however, for short time periods, it is difficult to separate SPE-induced changes from those caused by gravity waves, planetary waves, and other sources of natural variability that can cause larger variations.

Acknowledgments

Funding for C. Bardeen, C. Jackman, and D. Marsh is from the NASA Living With a Star Targeted Research and Technology program, grant 10-LWSTRT10-0109. Funding for C. Randall and M. Hervig is from the AIM program. AIM is funded by NASA through the Small Explorer program under contract NAS5-03132. The CIPS and SOFIE observations, including documentation and software for reading the data, are available at the AIM website, aim.hamptonu.edu. SOFIE data are also available at the GATS website, sofie.gats-inc.com. Model data will be made available upon request to bardeenc@ucar.edu. We thank the AIM mission operations and data processing teams for their excellent support. Computing resources supporting this work were provided by the NASA High-End Computing (HEC) Program through the NASA Advanced Supercomputing (NAS) Division at Ames Research Center. The CESM project is supported by the National Science Foundation and the Office of Science (BER) of the U.S. Department of Energy. NCAR is sponsored by the National Science Foundation.

References

Bardeen, C. G., O. B. Toon, E. J. Jensen, D. R. Marsh, and V. L. Harvey (2008), Numerical simulations of the three-dimensional distribution of meteoric dust in the mesosphere and upper stratosphere, *J. Geophys. Res.*, *113*, D17202, doi:10.1029/2007JD009515.

Bardeen, C. G., O. B. Toon, E. J. Jensen, M. E. Hervig, C. E. Randall, S. Benze, D. R. Marsh, and A. Merkel (2010), Numerical simulations of the three-dimensional distribution of polar mesospheric clouds and comparisons with Cloud Imaging and Particle Size (CIPS) experiment and the Solar Occultation For Ice Experiment (SOFIE) observations, *J. Geophys. Res.*, *115*, doi:10.1029/2009JD012451.

Becker, E. and C. von Savigny (2010), Dynamical heating of the polar summer mesopause induced by solar proton events. *J. Geophys. Res.*, *115*, D00I1, doi: 10.1029/2009JD012561.

Crutzen, P. J., I. S. A. Isaksen, and G. C. Reid (1975), Solar proton events: Stratospheric sources of nitric oxide, *Science*, *189*, 457–459, doi:10.1126/science.189.4201.457.

Dalin, P., et al. (2011), A comparison between ground-based observations of noctilucent clouds and Aura satellite data, *J. Atmos. Sol-Terr. Phys.*, *73*(14–15), 2097–2109, doi:10.1016/j.jastp.2011.01.020.

Garcia, R. R., D. R. Marsh, D. E. Kinnison, B. A. Boville and F. Sassi (2007), Simulation of secular trends in the middle atmosphere, 1950–2003, *J. Geophys. Res., 112*, D09301, doi:10.1029/2006JD007485.

Gordley, L. L., et al. (2009), The Solar Occultation For Ice Experiment (SOFIE), *J. Atmos. Sol. Terr. Phys.*, doi:10.1016/j.jastp.2008.07.012.

Hervig, M. E., M. H. Stevens, L. L. Gordley, and L. E. Deaver (2009a), Relationships between polar mesospheric clouds, temperature, and water vapor from Solar Occultation for Ice Experiment (SOFIE) observations, *J. Geophys. Res.*, *114*, doi:10.1029/2009JD012302.

Hervig, M. E., L. L. Gordley, L. E. Deavers, D. E. Siskind, M. H. Stevens, J. M. Russell III, S. M. Bailey, L. Megner, and C. G. Bardeen (2009b), First satellite observations of meteoric smoke in the middle atmosphere, *Geophys. Res. Letts.*, *36*, L18805, doi: 10.1029/2009GL039737.

Hurrell, J. W., et al. (2013), The community Earth system model: A framework for collaborative research, *Bull. Am. Meteorol. Soc.*, *94*, 1339–1360, doi:10.1175/BAMS-D-12-00121.1.

Jackman, C. H., R. G. Roble, and E. L. Fleming (2007), Mesospheric dynamical changes induced by the solar proton events in October–November 2003, *Geophys. Res. Lett.*, *34*, doi:10.1029/2006GL028328.

Jackman, C. H., et al. (2008), Short- and medium-term atmospheric constituent effects of very large solar proton events, *Atmos. Chem. Phys.*, *8*, 765–785, doi:10.5194/acp-8-765-2008.

Jackman, C. H., C. E. Randall, V. L. Harvey, S. Wang, E. L. Fleming, M. López-Puertas, B. Funke, and P. F. Bernath (2014), Middle atmospheric changes caused by the January and March 2012 solar proton events, *Atmos. Chem. Phys.*, *14*, 1025–1038, doi:10.5194/acp-14-1025.

Lamarque, J.-F., et al. (2011), CAM-chem: Description and evaluation of interactive atmospheric chemistry in CESM, *Geosci. Model Dev.*, *5*, 369–411, doi:10.5194/gmd-5-369-2012.

Lumpe, J. D., et al. (2013), Retrieval of polar mesospheric cloud properties from CIPS: Algorithm description, error analysis and cloud detection sensitivity, *J. Atmos. Sol. Terr. Phys.*, *104*, 167–196, doi:10.1016/j.jastp.2013.06.007.

Marsh, D. R., M. E. Mills, D. E. Kinnison, J.-F. Lamarque, N. Calvo, and L. M. Polvani (2013), Climate change from 1850 to 2005 simulated in CESM1 (WACCM), *J. Climate*, *26*, 7372–7391, doi:10.1175/JCLI-D-12-0558.1.

McClintock, W., D. W. Rusch, G. E. Thomas, A. W. Merkel, M. R. Lankton, V. A. Drake, S. M. Bailey, and J. M. Russell (2009), The cloud imaging and particle size experiment on the aeronomy of ice in the mesosphere mission: Instrument concept, design, calibration, and on-orbit performance, *J. Atmos. Sol. Terr. Phys.*, doi:10.1016/j.jastp.2008.10.011.

Merkel, A. W., G. E. Thomas, S. E. Palo, and S. M. Bailey (2003), Observations of the 5-day planetary wave in PMC measurements from the Student Nitric Oxide Explorer Satellite, *Geophys. Res. Lett.*, *30*, doi:10.1029/2002GL016524.

Rahpoe, N., C. von Savigny, C. E. Robert, M. T. DeLand, and J. P. Burrows (2011), Impact of solar proton events on noctilucent clouds, *J. Atmos. Sol. Terr. Phys.*, *73*, 2073–2081, doi:10.1016/j.jastp.2010.07.017.

Rapp, M., F.-J. Lübken, A. Müllemann, G. Thomas, and E. Jensen (2002), Small scale temperature variations in the vicinity of NLC: Experimental and model results, *J. Geophys. Res.*, *107*(D19), 4392, doi:10.1029/2001JD001241.

Rienecker, M.M., et al. (2008), The GEOS-5 data assimilation system—Documentation of versions 5.0.1, 5.1.0, and 5.2.0, *Tech. Rep. Ser. on Global Modeling and Data Assimilation,* 27.

Russell, J. M., et al. (2009), Aeronomy of Ice in the Mesosphere (AIM): Overview and early science results, *J. Atmos. Sol. Terr. Phys.*, doi:10.1016/j.jastp.2008.08.011.

Schwartz, M. J., et al. (2008), Validation of the Aura Microwave Limb Sounder temperature and geopotential height measurements, *J. Geophys. Res.*, *113*, D15S11, doi:10.1029/2007JD008783.

Solomon, S., and P. J. Crutzen (1981), Analysis of the August 1972 solar proton event including chlorine chemistry, *J. Geophys. Res.*, *86*, 1140–1146, doi:10.1029/JC086iC02p01140.

Swider, W., and T. J. Keneshea (1973), Decrease of ozone and atomic oxygen in the lower mesosphere during a PCA event, *Planet. Space Sci.*, *21*, 1969–1973.

Toon, O. B., R. P. Turco, D. Westphal, R. Malone, and M. S. Liu (1988), A multidimensional model for aerosols: Description of computational analogs, *J. Atmos. Sci.*, *45*(15), 2123–2143.

von Clarmann, T., et al. (2013), The solar proton events in 2012 as observed by MIPAS, *Geophys. Res. Letts.*, *40*, 2339–2343, doi:10.1002/grl.50119.

von Savigny, C., M. Sinnhuber, H. Bovensmann, J. P. Burrows, M. B. Kallenrode, and M. Schwartz (2007), On the disappearance of noctilucent clouds during the January 2005 solar proton events, *Geophys. Res. Letts.*, *34*, L02805, doi:10.1029/2006GL028106.

Weeks, L. H., R. S. Cuikay, and J. R. Corbin (1972), Ozone measurements in the mesosphere during the solar proton event of 2 November 1969, *J. Atmos. Sci.*, *29*, 1138–1142.

Winkler, H., C. von Savigny, J. P. Burrows, J. M. Wissing, M. J. Schwartz, A. Lambert, and M. García-Comas (2012), Impacts of the January 2005 solar particle event on noctilucent clouds and water at the polar summer mesopause, *Atmos. Chem. Phys.*, *12*, 5633–5646, doi:10.5194/acp-12-5633-2012.